Y. Mao & Y. Yang (2017) Backstepping sliding mode control of gridconnected inverters, International Journal of Electronics Letters, 5:3, 314-326, DOI: 10.1080/21681724.2016.1216174

To appear in the *International Journal of Electronics*
Vol. 00, No. 00, Month 20XX, 1–9

Design of a Robust Backstepping Sliding Mode Control For Grid-Connected Inverters

Yuan Mao[a] and Kaiyuan Wang[b*]

[a]*Department of Electrical Engineering, The Hong Kong Polytechnic University, Hong Kong*; [b]*Department of Electrical and Electronics Engineering, The University of Hong Kong, Hong Kong*

(*Received 00 Month 20XX; accepted 00 Month 20XX*)

For renewable energy systems, grid-connected inverters are widely adopted to convert energy to the power grids. However, considering the fluctuation of the renewable energy sources and the external signal disturbance on the control signal, the grid-connected inverters suffer from the bad performance of the waveform and possibility of instability when the inverters are controlled by the conventional PI control and sliding mode control (SMC). This paper presents a backstepping sliding mode (BSM) control, which can successfully eliminate the effect being caused by the fluctuation of renewable energy sources and the control signal disturbance from external signals. The stability can also be guaranteed when the grid-connected inverters are controlled by BSM controllers.

Keywords: renewable energy; grid-connected inverter; PI; sliding mode control; backstepping sliding mode; stability

1. Introduction

As the renewable energy like wind and solar energy are becoming popular around the world, the grid-connected inverters are widely adopted to convert energy from the renewable energy sources to the power grids, and vice versa (Iov, Blaabjerg, & Hansen, 2010; Veerachary, Senjyu, & Uezato, 2002). Besides, due to the intermittent nature of renewable energy sources, grid-connected inverters are extensively used as static var compensator (STATCOM), e.g. (Gyugyi, 1988), active power filter (APF), e.g. (Agaki, 2005), and electric spring (ES), e.g. (Hui, Lee, & Wu, 2012) to compensate active and reactive power for stabilizing the power grids. In various fields, different types of inverters, including single-phase voltage source inverter, single-phase current source inverter, three-phase voltage source inverter, three-phase current source inverter, and multiple phase inverter are used. However, the most fundamental one and people studied most is the single-phase voltage source grid-connected inverter, e.g. (Kamel & Ortmeyer, 2007; Rymarski, 2009; Trigg, Dehbonei, & Nayar, 2008). For the single-phase voltage source inverter, the classic control strategy is the two-loop PI control strategy, e.g. (Abdel-Rahim & Quaicoe, 1996; Arafat, Palle, & Husain, 2012; Eren, Pahlevani, Bakhshai, & Jain, 2014; Hinago

*Corresponding author. Email: yuan.my.mao@connect.polyu.hk

& Koizumi, 2009; Mao, Yang, Chen, & Wang, 2012). The outer PI control loop produces the reference signal for the inner PI control loop and the inner PI control loop is designed for fine regulation to improve the power quality. However, both loops of PI control are based on the linearized system and only designed for one operating point. Any large perturbation to the systems, like remarkable variation of the wind speed, prominent change of the light tensity, disturbance of the control signal, and drift of the parameters can lead to unsatisfactory steady and dynamic performances. Therefore, a variety of nonlinear control strategies are applied to substitute either one or both of the PI control loops, e.g. (Gudey, S. K. & Gupta, R., 2015; Ho & Chung, 2005; Wai, Lin, Huang, & Chang, 2012; Wai, Lin, Wu, & Huang, 2013; Yang & Smedley, 2008). In (Gudey, S. K. & Gupta, R., 2015; Wai, Lin, Huang, & Chang, 2012), sliding mode control (SMC) are adopted, which present more robust performance than the conventional PI. In (Wai, Lin, Wu, & Huang, 2013), with backstepping control, the output voltage of the inverter has better power quality than the one with conventional PI control. Even those proposed nonlinear control strategies have such merits, the performance is still inferior when the renewable energy source fluctuates too much and the control signal is disturbed externally. In this paper, the backstepping sliding mode (BSM) control is proposed to resolve such problems. With stability analysis, BSM in this paper is strictly designed. BSM shows its better stability performance over conventional PI and SMC when the dc voltage source of the grid-connected inverter fluctuates severely and the control signal is disturbed by simulation and experimental results. However, due to one more current sensor is needed for BSM, the cost of BSM is a little bit higher than SMC and PI, but the algorithm does not incremented a lot and can be implemented by the same type digital controller, e.g. TMS320F28069. The Complexity and dynamic response performance of BSM is almost the same as SMC. Both BSM and SMC are more complex than PI, but both of them have better dynamic response performance.

2. State-space model of the grid-connected inverter

The grid-connected inverter in this paper is implemented by the single-phase voltage source half-bridge inverter. The topology is depicted in Figure 1.

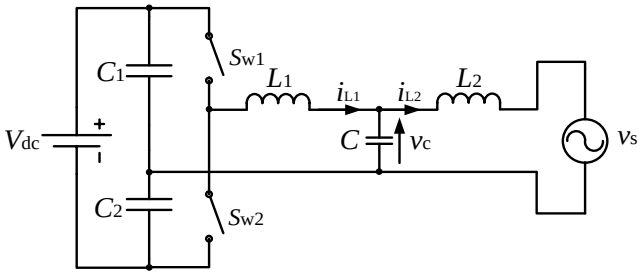

Figure 1. Simplified model of the grid-connected inverter implemented by a single-phase half-bridge inverter.

Regarding the inherent voltage balance of the DC capacitors C_1 and C_2, based on Kirchhoff's law, the state-space model of the grid-connected inverter, can be

obtained as

$$\begin{cases} \dfrac{di_{L1}}{dt} = -\dfrac{v_C}{L_1} + \dfrac{u}{2L_1}V_{\mathrm{dc}} \\ \dfrac{di_{L2}}{dt} = \dfrac{v_C}{L_2} - \dfrac{v_{\mathrm{s}}}{L_2} \\ \dfrac{dv_C}{dt} = \dfrac{i_{L1}}{C} - \dfrac{i_{L2}}{C} \end{cases}, \tag{1}$$

where i_{L1} is the current flowing through the inductor L_1, i_{L2} is the current flowing through the inductor L_2, v_C is the voltage over the capacitor C, V_{dc} is the voltage of the renewable energy source which can be directly dc voltage or dc voltage after rectification, and v_{s} is the voltage of the ac power grid. u is the control signal (modulation index) based on the fundamental frequency (50Hz).

Then, consider the fluctuation of renewable energy source $\widetilde{V_{\mathrm{dc}}}$ and the control signal disturbance $\widetilde{u}$, the first equation of (1) can be further written as

$$\frac{di_{L1}}{dt} = -\frac{v_C}{L_1} + \frac{u}{2L_1}V_{\mathrm{dc}} + f\left(t\right), \tag{2}$$

where

$$f\left(t\right) = \frac{V_{\mathrm{dc}}}{L_1}\widetilde{u} + \frac{u}{2L_1}\widetilde{V_{\mathrm{dc}}}. \tag{3}$$

3. Design of the BSM controller

Step 1: Define the tracking error of the voltage over the capacitor as

$$e_1 = v_{ref1} - v_c, \tag{4}$$

where v_{ref1} is the reference of capacitor voltage of LCL filter and its derivative as

$$\dot{e}_1 = \dot{v}_{ref1} - \dot{v}_c. \tag{5}$$

The Lyapunov function is defined as

$$V_1 = \frac{1}{2}e_1^2. \tag{6}$$

Then, a virtual reference for $\overline{i_{L1}}$ can be obtained as

$$\overline{i_{L1}} = i_{L2} + C\dot{v}_{ref1} + c_1 e_1, \tag{7}$$

where c_1 is a positive number.
Then, the derivative of V_1 can be obtained based on (1) as

$$\dot{V}_1 = e_1\dot{e}_1 = e_1\left(\dot{v}_{ref1} - \frac{i_{L1}}{C} + \frac{i_{L2}}{C}\right) = -c_1 e_1^2 \leq 0. \tag{8}$$

However, in order to prevent "explosion of terms" (Swaroop, Hendrick, Yip, & Gerdes, 2000), a low-pass filter is included in the design. Define the output of the low-pass filter is i_{ref2}, which is also the reference current of i_{L1}. Then,

$$\begin{cases} \tau_1 \dot{i}_{ref2} + i_{ref2} = \overline{i_{L1}} \\ i_{ref2}(0) = \overline{i_{L1}}(0) \end{cases}, \tag{9}$$

where τ_1 is the time constant, can be obtained.
Step 2: Same procedure for i_{L1}. Define

$$e_2 = i_{ref2} - i_{L1}, \tag{10}$$

and its derivative as

$$\dot{e}_2 = \dot{i}_{ref2} - \dot{i}_{L1}. \tag{11}$$

Combine the sliding mode control that the sliding surface is designed as

$$s = e_2 \tag{12}$$

and the Lyapunov function is defined as

$$V_2 = \frac{1}{2} e_2^2. \tag{13}$$

In order to make sure $\dot{V}_2 \leq 0$, based on (2), the equivalent control law is given as

$$u_{eq} = \frac{L_1}{V_{dc}} \left(\frac{v_C}{L_1} + \frac{V_{dc}}{2L_1} + \dot{i}_{ref2} - c_2 e_2 - \eta \mathrm{sgn}(e_2) \right), \tag{14}$$

where c_2 is a positive number.

4. Stability analysis of the controlled system

The error of the low-pass filter is defined as

$$y = i_{ref2} - i_{L1}. \tag{15}$$

Based on (9),

$$\dot{i}_{ref2} = -\frac{y}{\tau_1} \tag{16}$$

can be obtained.
Then,

$$\dot{y} = -\frac{y}{\tau_1} + B(e_1, e_2, y, \dot{v}_{ref1}), \tag{17}$$

where B is the function of e_1, e_2, y and $\dot{v}_{ref1}$ can be derived.
The upper bound of B is also defined as M, so that

$$\frac{B}{M} - 1 \leq 0. \tag{18}$$

Define the Lyapunov function

$$V = \frac{e_1^2}{2} + \frac{e_2^2}{2} + \frac{y^2}{2} = p, \tag{19}$$

where p is a positive number. Then,

$$\begin{aligned}
\dot{V} &= e_1\dot{e}_1 + e_2\dot{e}_2 + y\dot{y} \\
&= e_1\left(e_2 + y - c_1e_1\right) + e_2\left(f\left(t\right) - \eta\mathrm{sgn}\left(e_2\right) - c_2e_2\right) + y\left(-\frac{y}{\tau_1} + B\right) \\
&\leq \left|e_1\right|\left|e_2\right| + \left|e_1\right|\left|y\right| - c_1e_1^2 - c_2e_2^2 - \frac{y^2}{\tau_1} + \frac{B^2y^2+1}{2} \\
&\leq \frac{1}{2}\left(e_1^2 + e_2^2\right) + \frac{1}{2}\left(e_1^2 + y^2\right) - c_1e_1^2 - c_2e_2^2 - \frac{y^2}{\tau_1} + \frac{B^2y^2+1}{2} \\
&= \left(1 - c_1\right)e_1^2 + \left(\frac{1}{2} - c_2\right)e_2^2 + \left(\frac{B^2+1}{2} - \frac{1}{\tau_1}\right)y^2 + \frac{1}{2}
\end{aligned} \tag{20}$$

is derived.
Apparently, if

$$\begin{cases}
c_1 \geq 1 + r \\
c_2 \geq \dfrac{1}{2} + r \\
\dfrac{1}{\tau_1} \geq \dfrac{M^2}{2} + \dfrac{1}{2} + r
\end{cases} \tag{21}$$

is guaranteed, where r is a small positive number.
Then, considering (18),

$$\begin{aligned}
\dot{V} &\leq -re_1^2 - re_2^2 + \frac{B^2 - M^2}{2}y^2 + \frac{1}{2} \\
&\leq -2rV + \left(\frac{B^2}{M^2} - 1\right)\frac{M^2}{2}y^2 + \frac{1}{2} \\
&\leq -2rV + 1
\end{aligned} \tag{22}$$

can be obtained. According to (19),

$$r \geq \frac{1}{4p} \tag{23}$$

should be satisfied to guarantee $\dot{V} \leq 0$.

Therefore, as long as (21) is guaranteed, e_1 can converge to be arbitrarily small.

Table 1. Specifications of the grid-connected inverter in simulation.

Parameters	Values	Parameters	Values
L_1	500 μH	L_2	500 μH
C	13.2 μF	C_1	3000 μF
C_2	3000 μF	V_{dc}	400 V
v_s	$311\sin(100\pi t)$ V		

Table 2. Specifications of the PI controller, SMC, and BSM controller in simulation.

Parameters	Values	Parameters	Values
K_{p}	0.2	K_{i}	0.25
c	1×10^4	η	0.5
r	1.0	τ_1	0.01
c_1	1.0×10^4	c_2	4.0×10^4

5. Simulation results

The specifications of the grid-connected inverter in simulation are given in Table 1. Parameters of the PI controller, SMC and BSM controller for simulation are given in Table 2. The block diagrams of the grid-connected inverter controlled by PI, SMC, BSM are given in Figure 2. For PI control, the root mean square (RMS) value of the capacitor voltage v_c is acquired and regulated to track the reference voltage V_{ref}. The error between V_{ref} and V_c is controlled by PI controller and combined with the phase impact of v_s to form the modulation waveform. Then, the waveform is modulated by triangle waveforms to develop the driving signals for the grid-connected inverter. For SMC, the equivalent control signal is formulated by the error of v_{ref} and v_c, v_s, and the dc voltage V_{dc}. Then, the equivalent control signal of SMC is modulated by triangle waveforms to have the driving signals for the grid-connected inverter. For BSM, the equivalent control signal is formulated by eq. (14) and also modulated by triangle waveforms to have the driving signals for the grid-connected inverter.

5.1. *Comparisons of PI, SMC, BSM when V_{dc} fluctuates*

In practice, V_{dc} can be renewable energy sources, batteries, and dc grids. Thus, the fluctuation of V_{dc} can frequently happen which may severely affect the performance of the grid-connected inverter and cause the instability of the system. Figure 3 shows the comparisons of v_c, RMS of v_c, and i_{L2} between PI, SMC, and BSM when V_{dc} fluctuates variously. The seed of the V_{dc} variation is $\left[1, -5, 4, -2, -5, 5\right]$for every seconds. The practical V_{dc} in the system is $V_{dc\_p} = V_{dc}$ (Fundamental) $\times$ Seed $\times$ Variation (%) (Fundamental).

Figure 3 shows that v_c will fluctuate and RMS of v_c reaches the steady state with large overshoot if V_{dc} fluctuates with large steps when the grid-connected inverter is controlled by the PI controller. When the grid-connected inverter is controlled by the SMC, the fluctuation is much smaller and RMS of v_c reaches the steady state with smaller overshoot. However, if the grid-connected inverter is controlled by the BSM controller, v_c and RMS of v_c are kept at steady state.

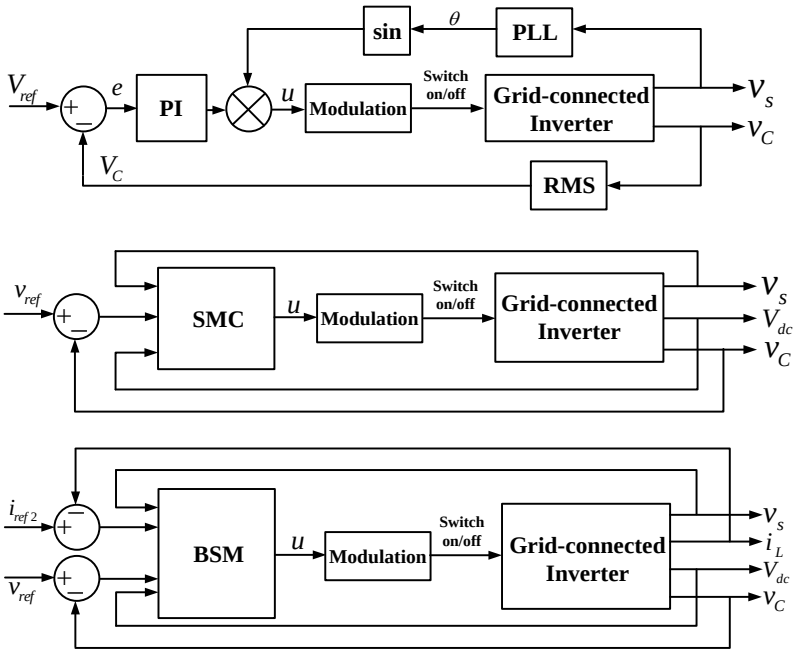

Figure 2. The block diagrams of the grid-connected inverter controlled by PI, SMC, and BSM.

5.2. *Comparisons of PI, SMC, BSM when the control signal is disturbed*

Comparisons of v_c, RMS of v_c, and i_{L2} between the PI, SMC, BSM when $\widetilde{u} = 0$, $\widetilde{u} = 0.25\sin(20\pi t)$, and $\widetilde{u} = 2.5\sin(20\pi t)$ are given in Figure 4. In Figure 4, as the disturbance on the control signal is stronger from (a) to (c), v_c fluctuates more, which leads to be unstable and RMS of v_c is severely distorted when the grid-connected inverter is controlled by PI controller. The performance of v_c and RMS of v_c are better when the system is controlled by SMC. However, if the disturbance is larger, the system will be unstable. However, v_c and RMS of v_c are kept at steady state when the BSM controller is adopted.

6. Experimental verification

The experiment is conducted on a TI's C2000$^{\text{TM}}$ Solar DC/AC voltage source inverter and Kikusui's PCR2000LE Power Supply. The photography of the experimental setup is shown in Figure 5. In the experiment, the single-phase half-bridge inverter is implemented by the TI's C2000$^{\text{TM}}$ Solar DC/AC voltage source inverter with IGBT of IRG4PC30FDPBf, 600 V IGBT drivers, differential circuits to sense the voltage of both V_{dc} and v_c, and a hall sensor to sense the inductor current i_{L1}. The DC voltage source with fluctuation is programmed on the Kikusui's PCR2000LE Power Supply. The AC grid is emulated by Triphase PM15F80C and the cable for the grid-connection, also known as the filter inductor L_2, is ASEA's inductor. The filter inductor L_1 and the filter capacitor C_1 of the LCL filter are internally installed in the inverter. The DSP used for the control is TI's F28069 Piccolo controlCARD. The specifications of the grid-connected inverter in experiment are given in Table 3. Parameters of the PI controller, SMC and BSM controller for experiment are given

Table 3. Specifications of the grid-connected inverter in experiment.

Parameters	Values	Parameters	Values
L_1	500 μH	L_2	500 μH
C	13.2 μF	C_1	3000 μF
C_2	3000 μF	v_s	$156\sin(100\pi t)$ V

Table 4. Specifications of the PI controller, SMC, and BSM controller in experiment.

Parameters	Values	Parameters	Values
K_{p}	0.2	K_{i}	0.25
c	1×10^4	η	0.5
r	1.0	τ_1	0.01
c_1	1.0×10^4	c_2	4.0×10^4

in Table 4. Figure 6 shows the comparisons of v_c and i_{L2} when V_{dc} fluctuates from 180 V to 200 V. In Figure 6(a), when the system is controlled by PI control with best tuning, v_c and i_{L2} take about 0.15 s to the new steady state. In Figure 6(b), when the system is controlled by SMC, v_c and i_{L2} take about 0.025 s to the new steady state. However, in Figure 6(c), when the system is controlled by BSM control, v_c and i_{L2} can almost reach the new steady state without transience. Apparently, BSM control have much better transient performance when V_{dc} fluctuates, which can guarantee the stability of the system in a wider operating range. Figure 7 shows the comparisons of v_c and i_{L2} when the equivalent control signal, which reflects the drift of parameters, is disturbed by several step pulses. When the system is controlled by PI control with best tuning, v_c and i_{L2} fluctuate intensively. When the system is controlled by SMC, v_c and i_{L2} have much better performance, but still a tender variation exists for both v_c and i_{L2}. When the system is controlled by BSM control, v_c and i_{L2} have no fluctuation. Apparently, BSM control is a very robust control.

7. Conclusion

The dc power source of the grid-connected inverter can be renewable energy sources, batteries and dc grids, which may fluctuate randomly. Besides, the control signal of the grid-connected inverter may also suffer from the disturbance from external signals. From simulation and experimental results, these two undesirable phenomena cannot be regulated well by conventional PI controller and SMC. However, if the fluctuation is too large and the control signal is severely disturbed, the system controlled by PI and SMC may lead to be unstable. In this paper, the proposed BSM can successfully eliminate the effect of the fluctuation of dc power source and the disturbance of the control signal. The grid-connected inverter controlled by BSM is stable and the waveform performance is acceptable. Besides, being compared with PI and SMC, although BSM requires more sensors, it is easy to be implemented by digital controllers. Hence, not too much additional hardware costs are needed for BSM. The dynamic response performance of BSM is almost the same as SMC, which is much better than PI.

References

Abdel-Rahim, N. M., & Quaicoe, J. E. (1996). Analysis and design of a multiple feedback loop control strategy for single-phase voltage-source UPS inverters. *IEEE Trans. Power Electron.*, *11*(4), 532–541.

Akagi, H. (2005). Active harmonic filters. *Proc. IEEE*, *93*(12), 2128–2141.

Arafat, M. N., Palle, S., Sozer, Y. & Husain, I. (2012). Transition control strategy between standalone and grid-connected operations of voltage-source inverters. *IEEE Trans. Ind. Appl.*, *48*(5), 1516–1525.

Eren, S., Pahlevani, M., Bakhshai, A., & Jain, P. (2014). An adaptive droop dc-bus voltage controller for a grid-connected voltage source inverter with LCL filter. *IEEE Trans. Power Electron.*, *30*(2), 547–560.

Gudey, S. K., & Gupta, R.(2015). Sliding-mode control in voltage source inverter-based higher-order circuits. *International Journal of Electronics*, *102*(4), 668–689.

Gyugyi, L. (1988). Power electronics in electric utilities: static var compensators. *Proc. IEEE*, *76*(4), 483–494.

Hinago, Y., & Koizumi, H. (2009). A single-phase multilevel inverter using switched series-parallel DC voltage sources. *IEEE Trans. Ind. Electron.*, *57*(8), 2643–2650.

Ho, B. M. T., & Chung, H. S. H. (2005). An integrated inverter with maximum power tracking for grid-connected PV systems. *IEEE Trans. Power Electron.*, *20*(4), 953–962.

Hui, S. Y. R., Lee, C. K., & Wu, F. F. (2012). Electric springs–A new smart grid technology. *IEEE Trans. Smart Grid*, *3*(3), 1552–1561.

Iov, F., Blaabjerg, F., & Hansen, A. D.(2010). Analysis of a variable-speed wind energy conversion scheme with doubly-fed induction generator. *International Journal of Electronics*, *90*(11), 779–794.

Kamel, A. M., & Ortmeyer, T. H. (2007). Harmonic reduction in single phase inverters using a parallel operation technique. *International Journal of Electronics*, *69*(3), 403–419.

Mao, H., Yang, X., Chen, Z., & Wang, Z. (2012). A hysteresis current controller for single-phase three-level voltage source inverters. *IEEE Trans. Power Electron.*, *27*(7), 3330–3339.

Rymarski, Z. (2009). Design method of single-phase inverters for UPS systems. *International Journal of Electronics*, *96*(5), 521–535.

Swaroop, D., Hendrick, J. K., Yip, P. P., & Gerdes, J. C. (2013). Dynamic surface control of a class of nonlinear systems. *IEEE Trans. Autom. Control*, *45*(10), 1893–1899.

Trigg, M. C., Dehbonei, H. & Nayar C. V. (2008). Digital sinusoidal PWMs for a microcontroller based single-phase inverter, Part 1: Principles of digital sinusoidal PWM generation. *International Journal of Electronics*, *95*(8), 819–840.

Veerachary, M., Senjyu, T., & Uezato, K. (2002). Neural network-based feedforward maximum power point tracking control for IDB converter-supplied PV system. *International Journal of Electronics*, *89*(5), 403–420.

Wai, R. J., Lin, C. Y., Huang, Y. C., & Chang, Y. R. (2012). Design of high-performance stand-alone and grid-connected inverter for distributed generation applications. *IEEE Trans. Ind. Electron.*, *60*(4), 1542–1555.

Wai, R. J., Lin, C. Y., Wu, W. C., & Huang, H. N. (2013). Design of backstepping control for high-performance inverter with stand-alone and grid-connected power-supply modes. *IET Power Electron.*, *6*(4), 752–762.

Yang, C., & Smedley, K. M. (2008). One-cycle-controlled three-phase grid-connected inverters and their parallel operation. *IEEE Trans. Ind. Appl.*, *44*(2), 663–671.

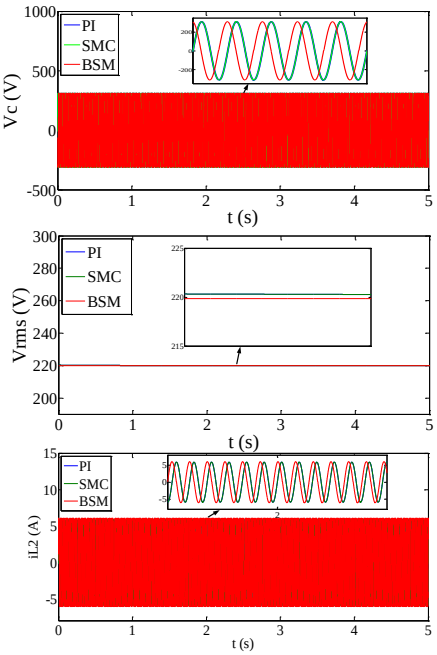

(a) 0% variation

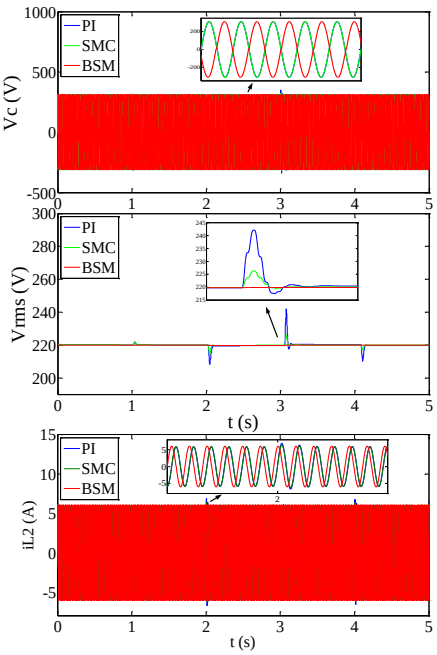

(b) 5% variation

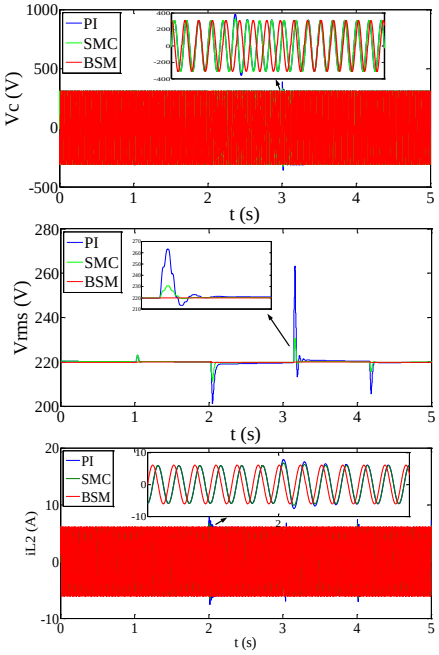

(c) 10% variation

Figure 3. Comparisons of v_c, RMS of v_c, and i_{L2} between the PI, SMC, BSM when V_{dc} has (a) 0% variation (b) 5% variation (c) 10% variation.

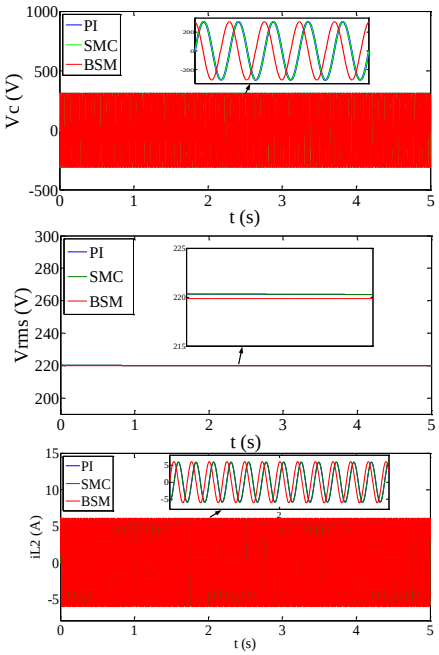

(a) $\widetilde{u} = 0$

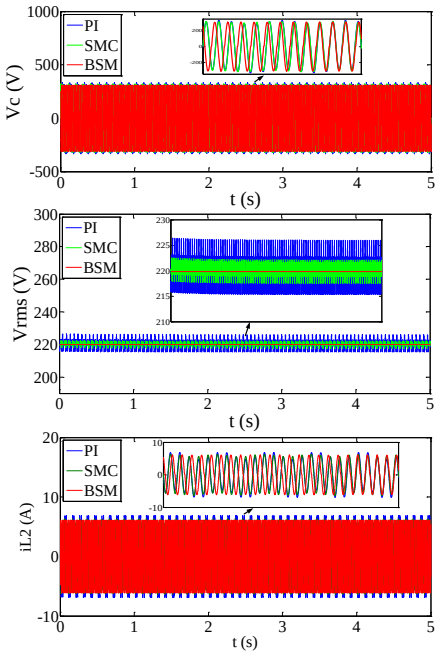

(b) $\widetilde{u} = 0.25\sin(20\pi t)$

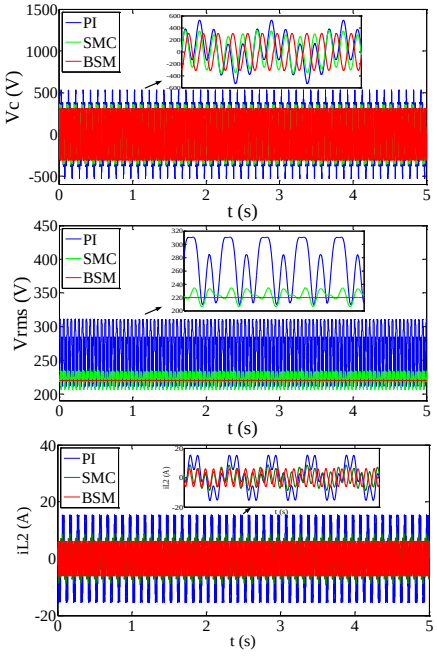

(c) $\widetilde{u} = 2.5\sin(20\pi t)$

Figure 4. Comparisons of v_c, RMS of v_c, and i_{L2} between the PI, SMC, BSM when (a) $\widetilde{u} = 0$ (b) $\widetilde{u} = 0.25\sin(20\pi t)$ (c) $\widetilde{u} = 2.5\sin(20\pi t)$.

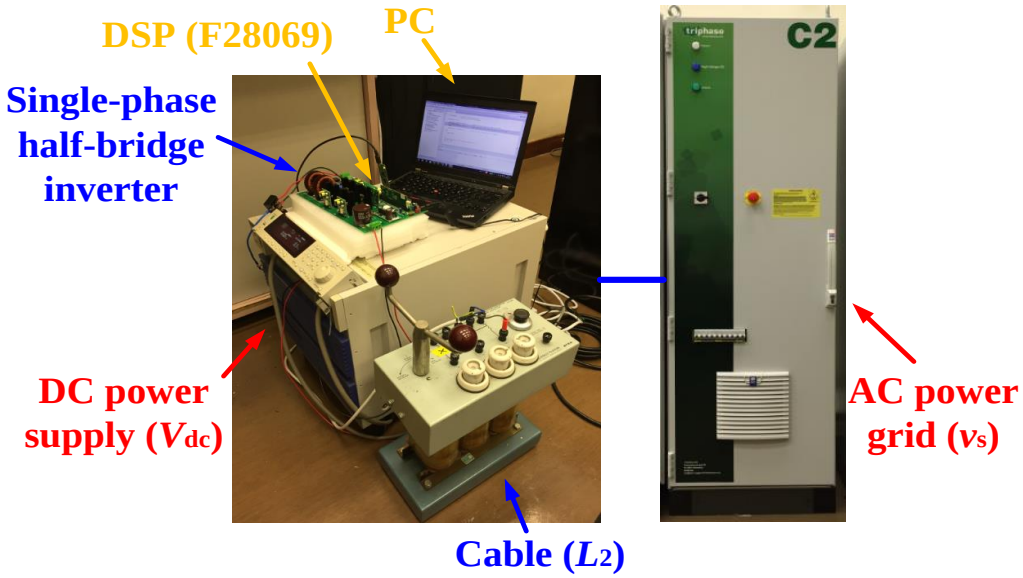

Figure 5. Photograph of the experimental setup.

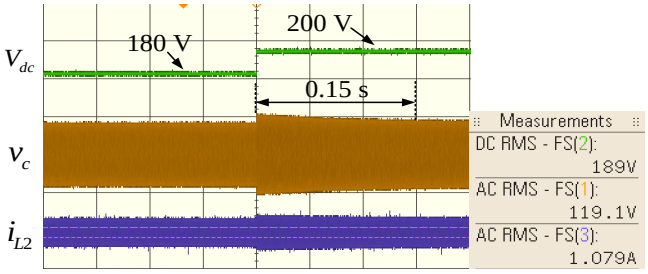

(a) PI control

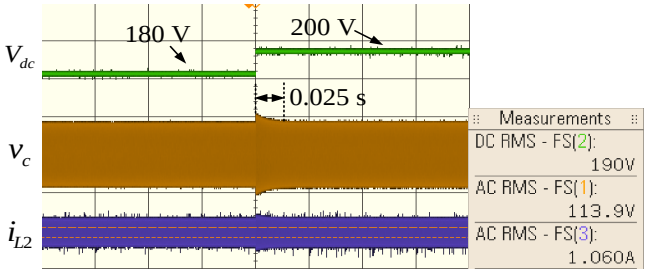

(b) SMC

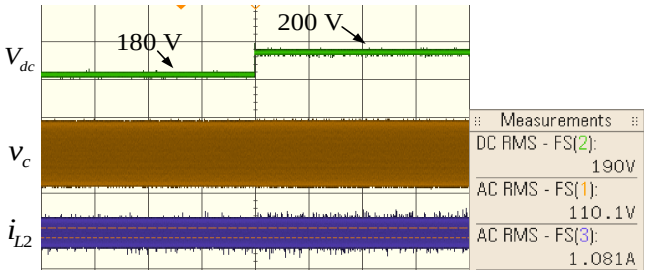

(c) BSM control

Figure 6. Comparisons of the system being controlled by PI control, SMC, and BSM control when V_{dc} fluctuates from 180 V to 200 V.

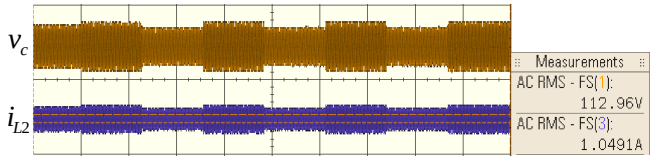

(a) PI control

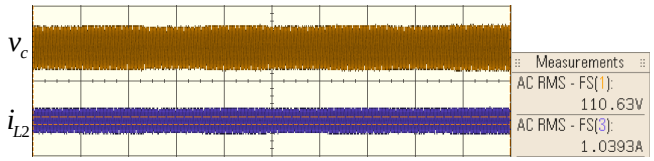

(b) SMC

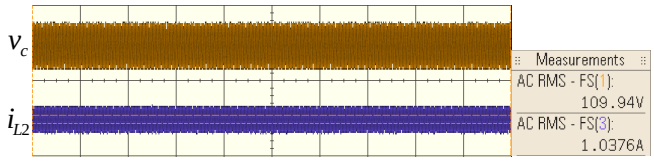

(c) BSM control

Figure 7. Comparisons of the system being controlled by PI control, SMC, and BSM control when the equivalent control signal is disturbed by step pulses.